Strain-induced metal-insulator transition in ultrathin films of SrRuO₃

Kapil Gupta,[*] Basudeb Mandal, and Priya Mahadevan[†]

Department of Condensed Matter Physics and Materials Science, S.N. Bose National Centre for Basic Sciences,
JD Block, Sector III, Salt Lake, Kolkata 700098, India

The ultrathin film limit has been shown to be a rich playground for unusual low-dimensional physics. Taking the example of SrRuO₃, which is ferromagnetic and metallic at the bulk limit, one finds that it becomes antiferromagnetic and insulating at the three-monolayers limit when grown on SrTiO₃. The origin of the insulating state is traced to strongly orbital-dependent exchange splittings. A modest compressive strain of 1% of the SrTiO₃ substrate is then found to drive the system into a highly confined two-dimensional 100% spin polarized metallic state. This metal-insulator transition driven by a modest strain could be useful in two-state device applications.

PACS number(s): 73.20.At, 75.70.−i

I. INTRODUCTION

The birth of modern day electronics began with semiconductor technology. However, as device dimensions are reaching limits where their operation is no longer feasible without losses, alternate materials are being investigated for new-generation electronics. Transition metal oxides are one such class of materials being explored as possible candidates [1,2]. In contrast to semiconductor heterostructures, here, the strongly coupled spin, charge, and lattice degrees of freedom lead to very diverse phenomena even with small deviations in the parameter space. One such parameter that has been used to tune the properties of transition metal oxides is strain [3–6], where in some instances one has been able to render nonmagnetic materials ferromagnetic [7–9], in certain others one is able to use strain to induce ferroelectricity [10–13] and so on. Another key parameter that controls the properties of the films has been the choice of the substrate. This can be used to tune a different crystal structure for the films grown on top than is usually favored [14]. The films then adopt the new crystal structure for few nanometers till one has strain relaxation that takes it to the crystal structure favored in the bulk.

In this work we consider the example of SrRuO₃. This is both metallic and ferromagnetic in the bulk. Since SrRuO₃ involves a 4d transition metal atom, which have wide bands, the expectation was that when ultrathin films were grown on a substrate, it would retain its metallicity down to the ultrathin limit. However, it was shown experimentally that below four monolayers of SrRuO₃, the system was insulating [15,16]. First-principles electronic structure calculations were found to support this view and showed that lattice distortions drove the insulating state at the three-monolayers limit [17]. In this work we consider the three monolayers limit and examine if one can retain metallicity and stop the metal to insulator transition by subjecting the films to compressive strain. This was indeed found to be the case and a modest compressive strain of 1% was found to be sufficient. The metallic state at the three-monolayers limit was found to be highly confined in

two dimensions and was found to be completely spin polarized, similar to what has been suggested in sandwich structures of SrTiO₃ and SrRuO₃ [18]. The insulating state obtained in the absence of any strain however, was found to have a surprising origin. The lattice distortions of the RuO₆ octahedra result in a level ordering in which the d_{xz}, d_{yz} orbitals are at a lower energy compared to the d_{xy} orbitals. Indeed we find such a level ordering in the majority spin channel when we examine the density of states. However, one finds a reversal of the level ordering in the down spin channel. This is traced to the differences in the exchange splitting between the d_{xy} and the d_{xz}/d_{yz} orbitals, which arises from the superlattice geometry that one has in which the d_{xy} orbitals have wider bands associated with them than the d_{xz} and d_{yz} orbitals. Under compressive strain one can change the relative contributions of the energy gain arising from hopping with respect to that from the intra-atomic exchange interaction. This can be used to control which orbital is occupied in the minority spin channel. This then has been used to bring a crossover to a spin polarized metallic state with the fourth electron occupying the d_{xz} and d_{yz} levels. In contrast to the work by Verrisimo-Alves *et al.* [18] who find the highly confined two-dimensional 100% spin polarized electron gas in superlattices of SrRuO₃/SrTiO₃, we find this effect with just one monolayer of SrO on top of the RuO₂ layer, i.e., the three-monolayers limit. So this demonstrates that the ultrathin limit serves as a playground for manipulating various atomic interaction strengths and allows one to arrive at unusual aspects of the electronic structure, which are not found in the bulk limit.

II. METHODOLOGY

The electronic structure of bulk as well as thin films of SrRuO₃ was calculated within a plane-wave projected augmented wave [19] implementation of density functional theory within Vienna *ab initio* simulation package (VASP) [20,21]. The generalized gradient approximation (GGA) with Perdew-Burke-Ernzerhof (PBE) functional was used to treat exchange correlation functional [22]. Correlation effects on Ru were treated within the GGA + U method using the formalism of Dudarev [23]. A value of $U = 2.5$ eV and $J = 0.4$ eV was applied on the Ru atom as deduced from the constrained random phase approximation [24] based formalism. In spite of the results being calculated from a first-principles estimate

————
[*]Present address: Indo-Korea Science and Technology Centre, Bangalore 560029, India and Jawaharlal Nehru Centre for Advanced Scientific Research, Bangalore 560064, India.

[†]Corresponding author: priya@bose.res.in

of U, we have varied U as well as the double counting scheme used to illustrate the sensitivity of the results to the choice of U. However, the constrained RPA determined value of U is able to reproduce various limits observed experimentally indicating the predictive power of the approach. A k-point mesh of $6 \times 6 \times 6$ and $6 \times 6 \times 2$ was used for the bulk and thin film calculations respectively. It was increased to $8 \times 8 \times 8$ and $8 \times 8 \times 2$ to calculate the density of states. In addition an energy cutoff of 400 eV was used for the kinetic energy of the plane waves included in the basis. Spheres of radii equal to 0.9 Å were used to calculate the Ru d projected partial density of states.

The experimental structure was taken for bulk $SrRuO_3$ [25] and the internal coordinates were optimized. In order to calculate the electronic structure of the ultrathin films of $SrRuO_3$, we considered a symmetric slab consisting of 15 layers of TiO_2 and SrO growing in the (001) direction. The in-plane lattice constant was kept fixed at the experimental lattice constant of $SrTiO_3$, which is 3.905 Å. This is smaller than the pseudocubic lattice constant of $SrRuO_3$ found to be 3.92 Å. The substrate lattice constant was varied to simulate the effects of strain. The substrate was taken to terminate with the TiO_2 surface on which SrO/RuO_2 layers were added alternately. A vacuum of 15 Å was used to minimize the interaction between images of the slab. As $GdFeO_3$ type of distortions are found in bulk $SrRuO_3$, we allowed for both rotations as well as tilts of the octahedra. Again, as in the case of the bulk calculations, here also the internal coordinates were optimized. Lattice mismatch with the substrate imposes a compressive strain of 0.4% on $SrRuO_3$ thin films. These films were also considered on 1% and 2% compressed $SrTiO_3$, which leads to 1.4% and 2.4% compressive strain on the thin films of $SrRuO_3$.

III. RESULTS AND DISCUSSION

A. Bulk SrRuO₃

$SrRuO_3$ is found to be ferromagnetic and metallic in the bulk and favors an orthorhombic unit cell. The orthorhombicity is driven by both $GdFeO_3$ rotations of the RuO_6 octahedra as well as the tilts [28]. Weak Jahn Teller effects were found to exist in bulk $SrRuO_3$ [29]. Before we examine the properties of $SrRuO_3$ in the thin film form, we first examine the bulk structure in our calculations. The ferromagnetic metallic unit cell is found to be the ground state in our calculations. Comparing the structural parameters of our optimized structure with experiment, we find that the calculations get the Ru-O bond lengths in reasonable agreement with experiment. The bond angles are found to be 158° in the ac plane, slightly underestimated from the experimental values which are found to be in the range 161°–163° as shown in Table I. The bond angles in the b direction are found to be underestimated by 3°–5° from the experimental values [25–27].

B. Two monolayers of SrRuO₃ on SrTiO₃

As discussed in Sec. II, two or more monolayers of $SrRuO_3$ are grown on $SrTiO_3$. The rotations of the successive octahedra stacked in the c direction in $SrTiO_3$ are out of phase and this has been included in the calculations. Additionally one finds

TABLE I. Ru-O bondlengths and Ru-O-Ru angles for the experimental and the theoretically optimized bulk $SrRuO_3$. The GGA + U [34] method has been used for the theoretical calculations with a U of 2.5 eV and a J of 0.4 eV.

	Experiment [25–27]	U = 2.5, J = 0.4 eV
	Bondlengths (Å)	
ac-plane	1.99/1.98	2.00/1.99
b-direction	1.98	1.99
	Angles (°)	
ac-plane	161.1° − 162.8°	158°
b-direction	163.1° 165.1°	160°

that the substrate imposes a tetragonal crystal structure on the $SrRuO_3$ overlayers. We first examine the case where we have two monolayers of $SrRuO_3$ grown on TiO_2 terminated $SrTiO_3$ substrates. Photoemission experiments indicate that these films are insulating [18], and our calculations also find them to be so. In order to examine the origin of the insulating state in our calculations, we examine the distortions of the RuO_5 motifs in our optimized unit cell. These are shown in Fig. 1. The distortions in the ab plane are found to consist of Ru-O bond lengths equal to 1.95 Å and 1.97 Å as shown in Fig. 1(a). The out-of-plane Ru-O bond length is found to be 2.15 Å, dramatically modified from the in-plane Ru-O bond lengths. This suggests that the surface RuO_2 layer is weakly
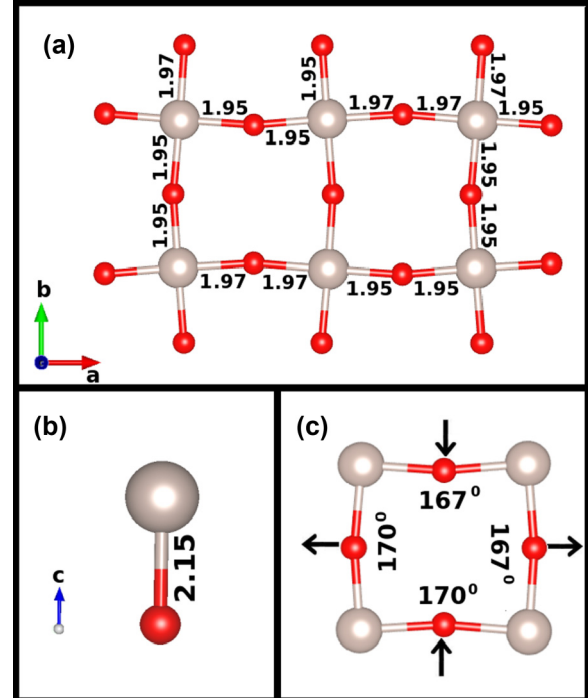

FIG. 1. (Color online) (a) The in-plane network of Ru (large gray spheres) and O (small red spheres) for two monolayers of $SrRuO_3$ grown on $SrTiO_3$ found in the GGA + U ($U = 2.5$ eV, $J = 0.4$ eV) calculations using the Dudarev [23] double counting scheme. The Ru-O bond lengths have also been shown in each case as well as (b) the out of plane Ru-O bond length and (c) the Ru-O-Ru angles. The direction of movement of the oxygen atoms are indicated by arrows.

coupled to the substrate. Further, the Ru environment is found to approach a square planar geometry. The large structural distortions observed here for the RuO_5 motifs would involve a large energy cost in terms of the strain energy in increasing the length of the Ru-O bond in the c direction. So, the natural question is to understand where the energy of this distortion is coming from and why it is happening in the first place. Ru in $SrRuO_3$ has a d^4 configuration. In early $3d$ transition metal oxides one has a smaller crystal field splitting than the exchange splitting. However for $4d$ oxides, one has a shorter exchange splitting than the crystal field splitting. This results in the Ru d states with t_{2g} symmetry being completely filled in the up spin channel and the fourth electron goes into the t_{2g} down spin channel. This is the energy level diagram for bulk $SrRuO_3$. At the two monolayers limit one has seen earlier [17] that the symmetry about the Ru site is reduced to square pyramidal. The level ordering is dictated by the long Ru-O bond in the z direction. We have the t_{2g} levels splitting into d_{xz} and d_{yz} at lower energies compared to the d_{xy} orbital. The orbitals with e_g symmetry split into the the d_{z^2} orbital at lower energy compared to the $d_{x^2-y^2}$ orbital. As a result we have the four electrons on Ru occupying the majority t_{2g}-derived orbitals and then the d_{z^2} orbital. Hence we have a rare occurrence of a high spin state at the Ru site. The gain in energy from the spin-state transition also explains why one can sustain the long Ru-O bond in the z direction.

Another puzzling aspect that we find is the polar nature of the distortions of the Ru-O bonds in the ab plane. This probably arises from the fact that the surface distortions have driven the system into a band insulator. The system can have weak second order Jahn-Teller effects and this is what we find here. The Ru atom is found off center towards a pair of oxygens in the ab plane and as a result a pair of oxygens have shorter Ru-O bond lengths of 1.95 Å than the other two (1.97 Å). The magnitudes of these distortions decrease when we include the tilts of the octahedra [30]. Additionally we find that the net electric polarization is zero as the dipole moments associated with different RuO_5 motifs are oriented in opposite directions. As discussed earlier, the Ru-O-Ru angles for bulk $SrRuO_3$ are found to be 158° for the in-plane case and 160° for the out-of-plane case. In the present case we find the bond angles equal to 167° and 170°. These deviations in the bond angles as large as 8°–10° from the values found for bulk $SrRuO_3$ are surprising, especially since compressive strain due to the substrate should result in shorter bonds and a more distorted Ru-O network. These expectations are based on our notional understanding of the origin of $GdFeO_3$ distortions. A smaller ion at the A site in a perovskite lattice of the form ABO_3, results in a smaller volume for the perovskite. This also leads to shorter bonds between the transition metal, B, and oxygen, which increases the repulsion between the electrons on B and oxygen. The structure, then distorts with the BO_6 octahedra rotating. This distortion, known as $GdFeO_3$ distortion is commonly observed in perovskite oxides, and leads to smaller B-O-B angles in the perovskite oxides with unit cell of smaller volume. The compressive strain of the substrate is expected to behave similarly. Contrary to these expectations, one instead finds an increase here. This could possibly arise from an attempt by the system to increase its bandwidth, as the effectively square planar geometry that is
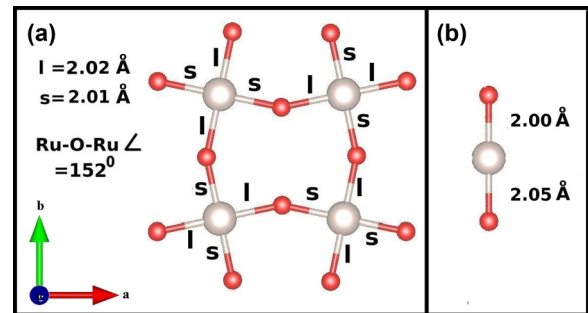

FIG. 2. (Color online) The in-plane Ru (large gray spheres) and oxygen (small red spheres) network showing Ru-O-Ru bond angles as well as Ru-O bond lengths for three monolayers of $SrRuO_3$ films grown on $SrTiO_3$ within our $GGA + U$ ($U = 2.5$ eV, $J = 0.4$ eV) calculations using the Dudarev double counting scheme.

favored leads to a further loss of bandwidth than linked RuO_5 motifs in the z direction.

C. Three monolayers of $SrRuO_3$ on $SrTiO_3$

Adding a layer of SrO on the two monolayers of $SrRuO_3$ results in the in-plane Ru-O network to adopt the structure shown in Fig. 2. Each Ru atom has a small Jahn-Teller distortion with the long and short Ru-O bonds differing by 0.01 Å. The in-plane Ru-O-Ru angles now at this limit of three monolayers are found to be 152°, 6°–8° less than the values found in bulk. This trend, however is expected in the case of compressive strain as discussed earlier. The out-of-plane bond lengths are found to be 2.0 Å and 2.05 Å. The longer Ru-O bond length in the z direction results in a degeneracy lifting of the t_{2g} orbitals with the d_{xz} and d_{yz} levels found at lower energies compared to the d_{xy} orbitals, as seen for the Ru d projected partial density of states for the up spin channel in Figs. 3(a)–3(e). However one finds a change in the level
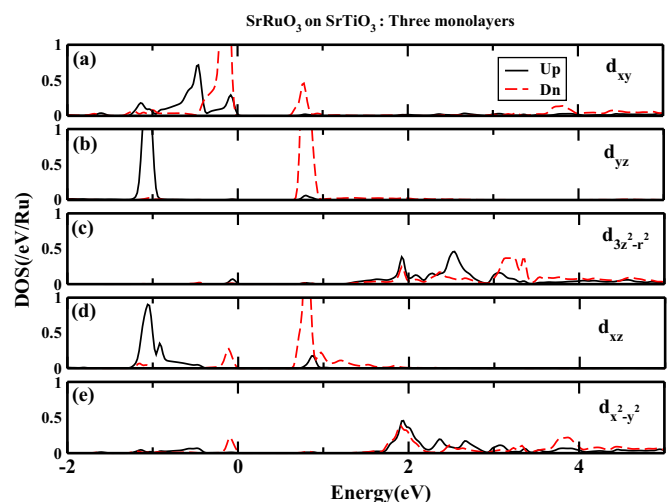

FIG. 3. (Color online) The up spin (solid line) as well as down spin (dashed line) orbital projected (a)–(e) Ru d partial density of states for three monolayers of $SrRuO_3$ grown on $SrTiO_3$ using the $GGA + U$ ($U = 2.5$ eV, $J = 0.4$ eV) method and the Dudarev double counting scheme. The zero of the energy scale is the Fermi energy.

ordering in the down spin channel. The fourth electron goes into the down spin d_{xy} orbital. This could be understood in terms of an orbital-dependent exchange splitting, the origin of which can be traced back to the itinerancy of the electron in the different d orbitals. The electron in d_{xy} orbitals delocalize in the xy plane forming wide bands, while those in the d_{xz} and d_{yz} orbitals couple via hopping with other d_{xz} and d_{yz} orbitals only along the x and y axis respectively and form narrower bands. The hopping in the z direction is very weak, as the corresponding Ti orbitals to which they can hop to are much higher in energy. As a result the exchange splitting for the d_{xy} orbitals is smaller than that of the d_{yz} and d_{xz} orbitals and hence the former gets occupied. This is shown schematically in Fig. 5(a). Thus the electronic structure brings out unusual aspects of the physics of this regime and enables us to manipulate interactions at the atomic level.

We then went on to examine whether the system would remain insulating under additional compressive strain. This was simulated by considering the compressed lattice parameter of the SrTiO$_3$ substrate, and subjecting it to 1% and 2% compressive strain. Considering the 1% strained case, we find the in-plane bond lengths to be 1.98 Åand 2.0 Åafter relaxation, while the out-of-plane bond lengths are found to be 2.07 Åand 2.04 Å along negative and positive z direction respectively. The in-plane bond angle is found to be 152.2°, smaller than the bulk value as expected. Examining the density of states [Figs. 4(a)–4(e)], we find that the level ordering in the majority spin channel is the same as when the substrate was unstrained, and we have d_{yz} and d_{xz} orbitals at lower energies compared to the d_{xy} orbital. The same level ordering is found in the down spin channel also and this is shown schematically in Fig. 5(b). This arises from the shorter Ru-O bonds that one has in the present case, which result in larger p-d hopping interaction strengths. Hence in the minority spin channel, the d_{xy} levels remain above the d_{xz} and d_{yz} levels. This results

FIG. 5. Schematic of level ordering in up (solid) and down (dashed) spin channel for SrRuO$_3$ on (a) SrTiO$_3$ and (b) 1% compressed SrTiO$_3$ within GGA $+ U$ ($U = 2.5$ eV, $J = 0.4$ eV) calculations using the Dudarev [23] double counting scheme.

in a metallic ground state [31]. For 2% compressed SrTiO$_3$ substrate, structure, and density of states remain the same qualitatively. In this case in-plane bond lengths are found to be 1.99 Å and 2.04 Å, while the out of plane bond lengths are found to be same as for the case of 1% compressed SrTiO$_3$. The in-plane angle is slightly reduced to 151.9° from 1% compressed case. This results in the same level ordering as the 1% compressed case.

Allowing for different magnetic configurations one finds that the ferromagnetic configuration is metallic while the antiferromagnetic solution is insulating. Comparing the energy in each case, one finds that the ferromagnetic solution has lower energy than the antiferromagnetic solution, though this would depend on the degree of localization. Interestingly as is evident from the charge density plotted for the energy interval from -1 eV to 0 eV, where 0 is the Fermi energy, one finds that this metallic state is strongly confined to just one monolayer (Fig. 6) and is in addition 100% spin polarized. This could
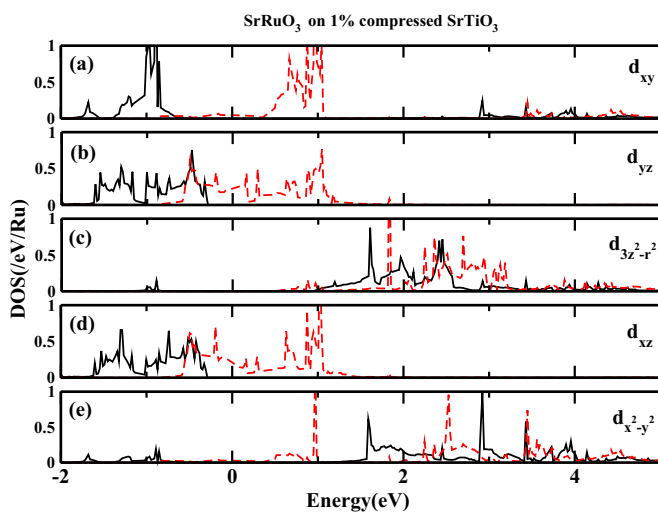

FIG. 4. (Color online) The up spin (solid line) as well as down spin (dashed line) orbital projected (f)-(j) Ru d partial density of states for three monolayers of SrRuO$_3$ grown on 1% compressed SrTiO$_3$ using the GGA $+ U$ ($U = 2.5$ eV, $J = 0.4$ eV) method and the Dudarev double counting scheme. The zero of the energy scale is the Fermi energy.
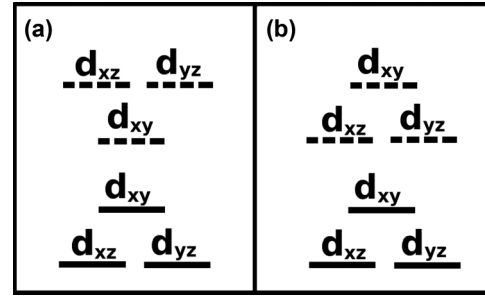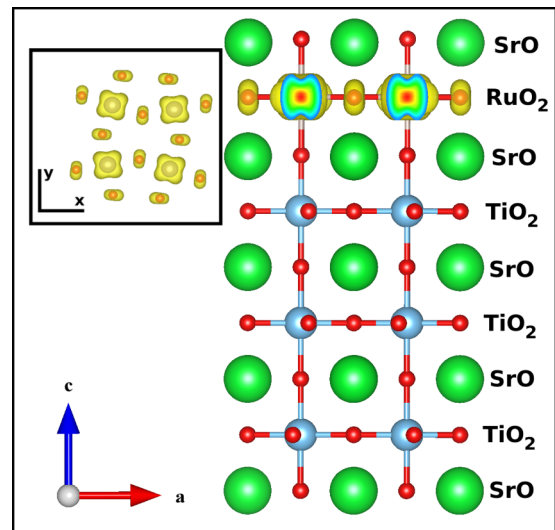

FIG. 6. (Color online) The layer-resolved charge density in the energy interval -1 eV to 0 eV (Fermi energy) for three monolayers of SrRuO$_3$ grown on 1% compressed SrTiO$_3$ within GGA $+ U$ ($U = 2.5$ eV, $J = 0.4$ eV) calculations using the Dudarev [23] double counting scheme. The view of the RuO$_2$ plane in the xy plane is shown in an inset.

have a lot of applications, one of them being in thermoelectrics as suggested by Ohta *et al.* [32]. Further the metal-insulator transition driven by a modest strain could have applications in two-state devices. The work by Verissimo-Alves *et al.* [18] found a spin-polarized strongly confined metallic state in heterostructures of $SrRuO_3$ and $SrTiO_3$. Here we show that just one monolayer of SrO is sufficient to result in this metallic state. The competing state with an energy 20 and 39 meV/Ru higher for the films grown on 1% and 2% compressed $SrTiO_3$ substrate is found to favor an antiferromagnetic solution. In this case, however, one finds that the d_{xz} and d_{yz} states are more localized. This drives a Jahn-Teller distortion in the system, with in-plane bond lengths now found to be equal to 1.98 Åand 2.0 Å. As a result one finds that the down spin d_{xz} orbital gets occupied at one site, while it is the d_{yz} orbital that is found to be occupied at the neighboring Ru site.

D. Four monolayers of $SrRuO_3$ on $SrTiO_3$

Again, examining the films grown on $SrTiO_3$ without the additional strain one finds that while the ground states were found to be insulating at the two and three monolayers limit, at the four monolayers limit, the system is found to be metallic. The surface RuO_2 layer has a similar ordering of levels [Figs. 8(a)–8(e)] as we found at the two-monolayers limit. One finds a high spin state is realized here also, though the layer is not insulating as we had earlier. A low density of states is found at the Fermi level here. The subsurface layer is found to exhibit stronger Jahn-Teller distortions than found for the three-monolayer case. As shown in the Fig. 7, the long and short in-plane Ru-O bonds are found to be 1.98 Å and 2.02 Å with the Ru-O-Ru angle now becoming $155°$. The reason for the more pronounced Jahn-Teller effect is easier to understand. Unlike in the three-monolayers limit, where the d_{yz} and d_{xz} orbitals on Ru have no states to interact with on Ti, the surface RuO_2 layer provides channels for the electrons on the subsurface d_{yz}, d_{xz} orbitals to delocalize. Hence there is no significant difference between exchange splittings of the d_{xy}, d_{yz}, and d_{xz} orbitals and so the scenario found at the three-monolayer limit does not happen here. So, as is shown
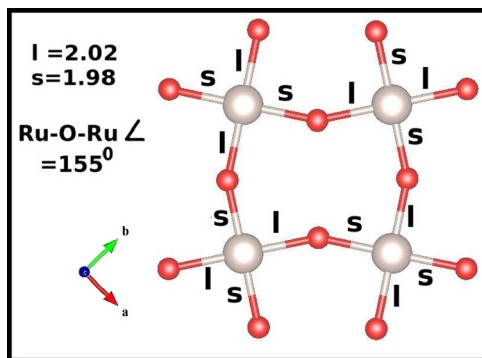

FIG. 7. (Color online) The Ru (large gray spheres) and oxygen (small red spheres) network of the subsurface layer for four monolayers of $SrRuO_3$ grown on $SrTiO_3$ using the GGA $+ U$ ($U = 2.5 \, eV, J = 0.4 \, eV$) method with the Dudarev [23] double counting scheme. The Ru-O bond lengths as well as the Ru-O-Ru bond angles are shown.
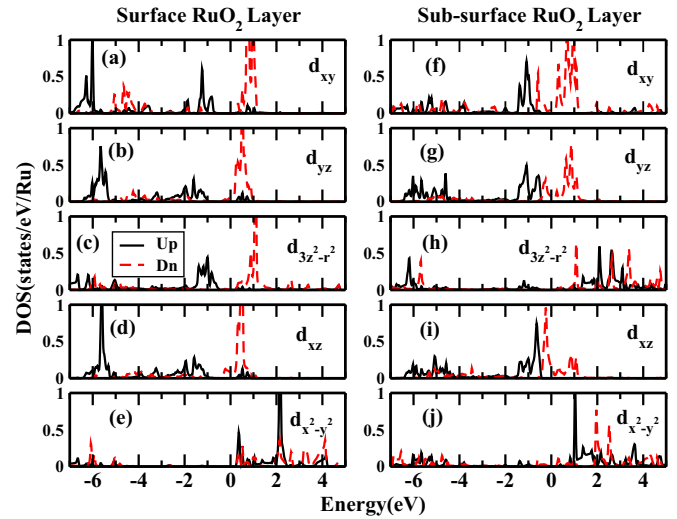

FIG. 8. (Color online) The up spin (solid line) as well as down spin (dashed line) orbital projected Ru d partial density of states for four monolayers of $SrRuO_3$ grown on $SrTiO_3$ for the surface RuO_2 layer (a)–(e) as well as for the subsurface RuO_2 layer (f)–(j) using the GGA $+ U$ ($U = 2.5 \, eV, J = 0.4 \, eV$) method and the Dudarev [23] double counting scheme. The zero of the energy scale is the Fermi energy.

in the Figs. 8(f)–8(j), after the t_{2g} up spin orbitals get occupied the fourth electron goes into the d_{xz} while the neighboring Ru has d_{yz} occupied. However the Jahn-Teller distortion is not large enough to make the system insulating.

E. Magnetism at the ultrathin limit

In Table II, we give the relative magnetic stabilization energies for the calculations corresponding to two, three, and four monolayers of $SrRuO_3$ on $SrTiO_3$. These have been given for the cases when we allowed $GdFeO_3$ rotations of the RuO_6 octahedra as well as the case when we had both $GdFeO_3$ rotations as well as the tilts of the octahedra. At the two-monolayer limit the system is found to be an antiferromagnetic insulator and inclusion of the tilts changes the stabilization energy only slightly. Similar trends are seen at the three-monolayer limit also, and the system remains to be antiferromagnetic. At the four-monolayer limit, an analysis of the density of states shows drastic differences between the

TABLE II. Total energies in meV/Ru for all magnetic configurations for two, three and four monolayers of $SrRuO_3$ grown on $SrTiO_3$ using GGA $+ U$ exchange correlation functionals and the Dudarev [23] double counting scheme.

		$GdFeO_3$ rotations	$GdFeO_3$+001 rotations
two-mono	FM	0	0
	AFM	−175	−157
three-mono	FM	0	0
	AFM	−45	−35
four-mono	FM	0	0
	AFM	−69	−110
	FM-AFM	−82	−129

TABLE III. Total energies in meV/Ru for all magnetic configurations for two and three monolayers of $SrRuO_3$ grown on $SrTiO_3$ with LDA/GGA for the exchange correlation functional and the double counting scheme as indicated.

		Two monolayers				
	U (eV)	0.0	1.0	2.0	2.5	3.0
LDA + U [23]	FM	0	0	0	0	0
	AFM	8	−93	−85	−57	348
	U (eV)	0.0	1.0	2.0	2.5	3.0
LDA + U [33]	FM	0	0	0	0	0
	AFM	8	−96	−19	−134	358
		Two monolayers				
		U (eV)	1	2.5	4	
GGA + U [33]		FM	0	0	0	
		AFM	55	−568	−1168	
		Three monolayers				
		U (eV)	1	2.5	4	
GGA + U [33]		FM	0	0	0	
		AFM	303	−96	−180	

surface and the subsurface electronic structure. The former is barely metallic with low density of states at the Fermi level and therefore favors an antiferromagnetic arrangement of the Ru spins. The subsurface, however has a ferromagnetic arrangement of the Ru spins, leading to a configuration labeled as FM-AFM in Table II and seems to be progressing towards the bulk electronic and magnetic structure.

In every case we have examined the dependence of U on the choice of exchange correlation functional as well as the type of double counting scheme used. LDA calculations are found to underestimate the distortions at the two-monolayers limit. At the two-monolayers limit using LDA we found an antiferromagnetic solution for small values of U, however one gets a ferromagnetic solution at large values of U as shown in Table III. We also examined the role of the double counting when using GGA + U exchange correlation functionals for both the two- and three-monolayers cases. Both at the two-monolayers limit and the three-monolayers limit one finds a ferromagnetic solution at lower values of U as the ground state and an antiferromagnetic solution as the ground state at larger values of U. For both LDA and GGA functionals, the different double counting schemes do not have a significant effect on the results. These results emphasize the sensitivity of the conclusions to the value of U. The constrained RPA determined U is able to reproduce the insulating ground state observed at the few-monolayers limit [15,16] as well as explain the exchange bias effects observed experimentally [16].

IV. CONCLUSION

We have examined the electronic structure of ultrathin films of $SrRuO_3$ grown on $SrTiO_3$. This limit turns out to be a strong playground of atomic physics with the three monolayers becoming insulating as a result of orbital-dependent exchange splittings. At the four-monolayers limit, one finds that the subsurface layer, which should be more delocalized than the three-monolayers limit has larger Jahn-Teller distortions, though the system becomes metallic. Subjecting the $SrRuO_3$ overlayers to an additional compressive strain by straining the substrate, one finds an insulator-metal transition at the three-monolayers limit, which results in a 100% spin-polarized electron gas, which is also highly confined.

[1] A. Ohtomo, D. A. Muller, J. L. Grazul, and H. Y. Hwang, Nature (London) **419**, 378 (2002).

[2] A. Ohtomo and H. Y. Hwang, Nature (London) **427**, 423 (2004).

[3] M. Dawber, K. M. Rabe, and J. F. Scott, Rev. Mod. Phys. **77**, 1083 (2005).

[4] V. Laukhin, V. Skumryev, X. Martí, D. Hrabovsky, F. Sánchez, M. V. García-Cuenca, C. Ferrater, M. Varela, U. Lüders, J. F. Bobo, and J. Fontcuberta, Phys. Rev. Lett. **97**, 227201 (2006).

[5] C. Thiele, K. Dörr, O. Bilani, J. Rödel, and L. Schultz, Phys. Rev. B **75**, 054408 (2007).

[6] A. D. Rata, A. Herklotz, K. Nenkov, L. Schultz, and K. Dörr, Phys. Rev. Lett. **100**, 076401 (2008).

[7] D. Fuchs, C. Pinta, T. Schwarz, P. Schweiss, P. Nagel, S. Schuppler, R. Schneider, M. Merz, G. Roth, and H. v. Löhneysen, Phys. Rev. B **75**, 144402 (2007).

[8] D. Fuchs, E. Arac, C. Pinta, S. Schuppler, R. Schneider, and H. V. Löhneysen, Phys. Rev. B **77**, 014434 (2008).

[9] K. Gupta and P. Mahadevan, Phys. Rev. B **79**, 020406(R) (2009).

[10] S. Bhattacharjee, E. Bousquet, and P. Ghosez, Phys. Rev. Lett. **102**, 117602 (2009).

[11] C. J. Fennie and K. M. Rabe, Phys. Rev. Lett. **97**, 267602 (2006).

[12] J. H. Lee and K. M. Rabe, Phys. Rev. Lett. **104**, 207204 (2010).

[13] J. H. Lee and K. M Rabe, Phys. Rev. Lett. **107**, 067601 (2011).

[14] A. T. Zayak, X. Huang, J. B. Neaton, and K. M. Rabe, Phys. Rev. B **74**, 094104 (2006).

[15] D. Toyota, I. Ohkubo, H. Kumigashira, M. Oshima, M. Lipmaa, M. Takizawa, A. Fujimori, K. Ono, M. Kawasaki, and H. Koinuma, Appl. Phys. Lett. **87**, 162508 (2005).

[16] J. Xia, W. Siemons, G. Koster, M. R. Beasley, and A. Kapitulnik, Phys. Rev. B **79**, 140407(R) (2009).

[17] P. Mahadevan, F. Aryasetiawan, A. Janotti, and T. Sasaki, Phys. Rev. B **80**, 035106 (2009).

[18] M. Verissimo-Alves, P. Garcia-Fernandez, D. I. Bilc, P. Ghosez, and J. Junquera, Phys. Rev. Lett. **108**, 107003 (2012).

[19] P. E. Blochl, Phys. Rev. B **50**, 17953 (1994); G. Kresse and D. Joubert, *ibid.* **59**, 1758 (1999).

[20] G. Kresse and J. Furthmüller, Phys. Rev. B **54**, 11169 (1996).

[21] G. Kresse and J. Furthmüller, Comput. Mat. Sci. **6**, 15 (1996).

[22] J. P. Perdew, in *Electronic Structure of Solids*, edited by P. Ziesche and H. Eschrig (Akademie Verlag, Berlin, 1991), p. 11.

[23] S. L. Dudarev, G. A. Botton, S. Y. Savrasov, C. J. Humphreys, and A. P. Sutton, Phys. Rev. B **57**, 1505 (1998).

[24] F. Aryasetiawan, M. Imada, A. Georges, G. Kotliar, S. Biermann, and A. I. Lichtenstein, Phys. Rev. B **70**, 195104 (2004).

[25] S. N. Bushmeleva, V. Yu. Pomjakushin, E. V. Pomjakushina, D. V. Sheptyakov, and A. M. Balagurov, Jour. Mag. Mag. Materials **305**, 491 (2006).

[26] M. Shikano, T. K. Huang, Y. Inaguma, M. Itoh, and T. Nakamura, Sol. Stat. Comm. **90**, 115 (1994).

[27] H. Kobayashi, M. Nagata, R. Kanno, and Y. Kawamoto, Mat. Res. Bull. **29**, 1271 (1994).

[28] J. M. Kiat and T. Roisnel, J. Phys. Cond. Mat. **8**, 3471 (1996).

[29] H.-T. Jeng, S.-H. Lin, and C.-S. Hsue, Phy. Rev. Lett. **97**, 067002 (2006).

[30] A. J. Hatt, N. A. Spaldin, and C. Ederer, Phys. Rev. B **81**, 054109 (2010).

[31] It should be noted that these calculations are not usually capable of capturing the paramagnetic metallic state but are very successful in capturing magnetic ground states.

[32] H. Ohta, S. Kim, Y. Mune, T. Mizoguchi, K. Nomura, S. Ohta, T. Nomura, Y. Nakanishi, Y. Ikuhara, M. Hirano, H. Hosono, and K. Koumoto, Nature Mat. **6**, 129 (2007).

[33] A. I. Liechtenstein, V. I. Anisimov, and J. Zaanen, Phys. Rev. B **52**, R5467(R) (1995).

[34] L. Wang, T. Maxisch, and G. Cener, Phys. Rev. B **73**, 195107 (2006).